High-Performance Hybrid Solar Cell Made from CdSe/CdTe Nanocrystals Supported on Reduced Graphene Oxide and PCDTBT

Shi Wun Tong, Nimai Mishra, Chen Liang Su, Venkatram Nalla, Wenya Wu, Wei Ji, Jie Zhang, Yinthai Chan, and Kian Ping Loh**

Core/shell tetrapods synthesized from CdSe and CdTe exhibit a type II band offset that induces separation of charge upon photoexcitation and localizes carriers to different regions of the tetrahedral geometry. CdSe/CdTe nanocrystals immobilized on oleylamine-functionalized reduced graphene oxide (rGO) sheets can be homogeneously mixed with an organic dye (PCDTBT) to form donor–acceptor dispersed heterojunctions and exhibit a high power conversion efficiency of ~3.3% in solar cell devices. The near-IR light absorbing type II nanocrystals complement the absorption spectrum of the visible light-absorbing organics. The high efficiency is attributed to the amine-functionalized rGO sheets, which allow intimate contact with the nanocrystals and efficient dispersal in the organic matrix, contributing to highly efficient charge separation and transfer at the nanocrystal, rGO, and polymer interfaces.

1. Introduction

Type II core/shell semiconductor nanocrystals have the potential to be excellent photoactive components owing to their infrared light harvesting properties, ultrafast photoinduced charge separation and long carrier lifetime.[1] However, application of these nanocrystals in photovoltaic applications is severely limited by the propensity for carriers to be trapped in the core, as well as the lack of an efficient charge percolation pathway towards the electrodes. It is well known that charge transport in a network of nanocrystals is governed by hopping or tunneling mechanisms. High loading of nanocrystals is thus necessary owing to its high percolation threshold (>30%), but excessive volume fraction increases the risk of aggregation. A layer-by-layer assembly of 6–9 layers of PbS nanocrystals was required to generate a device efficiency of 5.5%.[2]

One question is whether the nanocrystals can be immobilized on a conducting platform in order to prevent aggregation and improve their charge transport properties. It will be ideal if such a platform can be solution-processed and mixed with an organic dye. Reduced graphene oxide (rGO)[3] sheets generated from the chemical reduction of exfoliated graphite oxide sheets are excellent conductive additives and buffer carriers in a wide range of composites. In rGO, the functional groups residing on the basal plane (epoxy and hydroxyl groups) and edge (carboxylic acids group) can act as anchor sites for inorganic nanocrystals and prevent their aggregation. The use of a conductive matrix like rGO in a photoactive system has been known to enhance photoinduced charge transfer and charge collection, especially in photodetector devices,[4] but there are few reports of high efficiency solar cell devices using rGO-nanocrystal hybrids as the photoactive material. For example, the deposition of CdSe quantum dots on graphene sheets induces a high electron transfer constant of 3.6×10^8 s^{-1} but the solar cell device efficiency is still limited to 0.6%.[5] The low efficiency may be attributed to the absence of an energy matching or compatible electron donor system. To date, the most promising solution processable donors are polymers with high hole mobility, low bandgap and deep HOMO levels. Different polymer donors have been applied to complement the solar cell performance with nanocrystals[6–8] or rGO.[9,10] However, there are inherent processing problems to fabricate high efficiency devices using rGO and such polymers owing to their solvent incompatibility. The incorporation of organic-soluble polymer with sparingly soluble rGO is unlikely to generate the nanometer-scaled phase separation needed for good photovoltaic performance.[11] Limited by these factors, the best reported efficiency attained from hybrid devices to date based on graphene oxide derivatives and poly(3-hexylthiophene-2,5-diyl) (P3HT) or poly[2-methoxy-5-(3′,7′-dimethyloctyloxy)-1,4-phenylenevinylene] (MOMO-PPV) is around ~1.51%.[10]

Dr. S. W. Tong, Dr. C. L. Su, Prof. K. P. Loh
Graphene Research Centre
Department of Chemistry
National University of Singapore
3 Science Drive 3, 117543, Singapore
E-mail: chmlohkp@nus.edu.sg
Dr. N. Mishra, W. Wu, Prof. Y. Chan
Department of Chemistry
National University of Singapore
3 Science Drive 3, 117543, Singapore
E-mail: chmchany@nus.edu.sg
Dr. V. Nalla, Prof. W. Ji
Department of Physics
National University of Singapore
3 Science Drive 3, 117543, Singapore
Dr. J. Zhang
Institute of Materials Research and Engineering
3 Research Link, Singapore, 117602, Singapore

DOI: 10.1002/adfm.201303010

Here, we have successfully devised a strategy to integrate inorganic nanocrystals, rGO and polymer together to make a high performance inorganic-organic hybrid photovoltaic cell. Homogeneous mixing of the photoactive components is achieved by chemical treatment of the components with amines to ensure compatibility of the interfaces. Amine treatment of rGO and nanocrystals not only enhances their solubility in 1,2-dichlorobenzene (ODCB), but also produces a uniform anchorage of nanocrystals on rGO. By simply mixing the tetrapod-decorated rGO sheets with polymer as a single photoactive layer, a twofold increment of the power conversion efficiency (PCE) can be achieved over either polymer-rGO, polymer-nanocrystal or nanocrystal-rGO devices. The outstanding performance of this integrated photoactive system is attributed to the complementary light harvesting and efficient charge separation and transport at the dispersed heterojunctions of polymer/rGO, polymer/nanocrystal and nanocrystal/rGO.

2. Results and Discussion

Long range photoinduced charge separation in type II nanocrystals had been demonstrated to have potential photovoltaic applications.[12] Tetrapod shaped nanocrystals with CdSe core/CdTe branches present a staggered band alignment (type II) which favors spatial separation of hole and electron across the interfaces efficiently.[13] In particular, the branched morphology of the tetrapod affords better charge transport than spherical nanocrystals. Sensitizing conjugated polymers with these infrared active nanocrystals supported on rGO provides a spectrally tunable means of accessing the infrared while maintaining the advantageous properties of polymers.

CdSe/CdTe tetrapods were synthesized using a previously reported "seeded growth method" where the heteroepitaxial growth of Cd and Te precursors occurred on the facets of a CdSe core in order to achieve a branched geometry.[14] It is vital to produce zinc blende (ZB) CdSe since it will present four available (100) facets which act as sites for the growth of four CdTe arms to produce the tetrapod structure. To stabilize the ZB phase against conversion to the more thermodynamically stable hexagonal wurtzite phase, a lower injection temperature (~340 °C) was needed as compared to conventional methods.[14] In this case, we used a mixture of oleic acid, n-hexylphosphonic acid (HPA) and n-octadecylphosphonic acid (ODPA) as the ligand system. Transmission electron microscope (TEM) imaging (**Figure 1**a) of the synthesized products shows that a very high yield of tetrapods (90% with respect to nanorod, bipod and tripod by-products) can be obtained by this method, which may be attributed to the stabilization of the ZB phase of CdSe by oleic acid. Further ligand exchange with oleylamine was carried out to attain amine-capped tetrapods with core diameter of 7 nm and branch lengths in the range of 30–35 nm, as shown in the enlarged TEM image (Figure 1b).

Oleylamine is a typical surface modifier commonly used to improve the hydrophobic properties of nanostructures.[15] Due to the presence of oxygen functionalities on rGO, it can form an acid-base complexation with oleylamine, which improves its solubility in organic solvent (>5 mg/mL). The presence of amine groups in the amine-treated rGO has been verified by

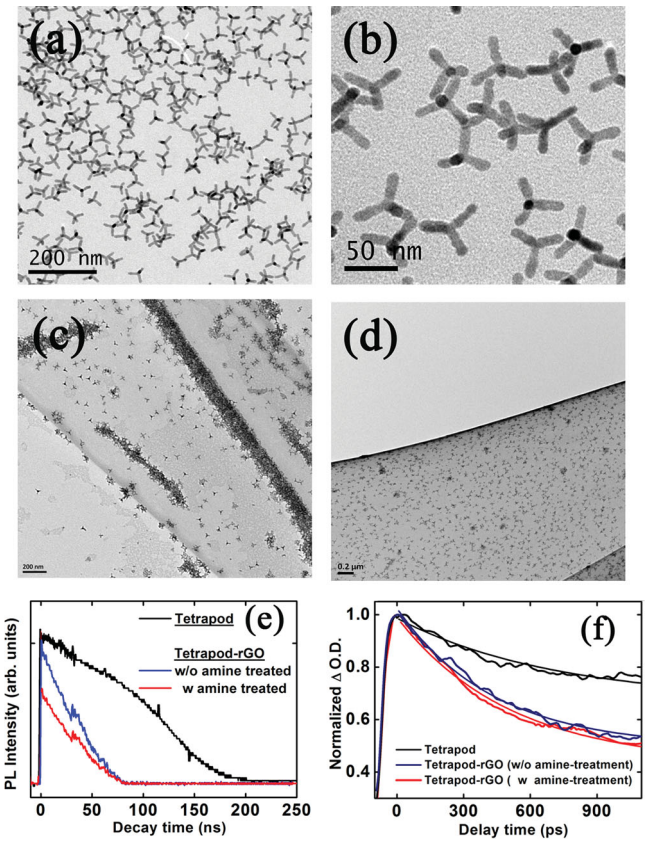

Figure 1. TEM images showing (a) homogeneous dispersion of the tetrapod-shaped nanocrystals in high yield (~90% yield); (b) magnified view showing the nanocrystals which consist of a CdSe core enclosing four CdTe arms. SEM images showing (c) aggregation of nanocrystals on untreated rGO; (d) same as (c) but with amine treatment. (e) Photoluminescence (PL) decay profiles showing that amine treatment leads to more effective quenching. The sharp spikes in the spectra are due to the laser noise. (f) Normalized decay profiles of Tetrapod, Tetrapod-rGO with and without oleylamine treatment probed at 800 nm. The data was fitted using a single exponential function.

FTIR (Supporting Information). The oleylamine treatment also plays an important role in immobilizing the tetrapods on rGO. The hydrophobic interaction between the aliphatic chains of oleylamine-functionalized rGO and the oleylamine ligands of CdSe/CdTe tetrapods enables good dispersion of the tetrapods on the rGO surface. This phenomenon is similar to the non-covalent binding of amine-capped nanoparticles on carbon nanotubes.[16] SEM images display a clear contrast in the attachment of tetrapods on rGO and amine-treated rGO as shown in Figure 1c and d respectively. Without the amine treatment, the majority of the tetrapods had aggregated (Figure 1c).

The amine-treated tetrapod-rGO network was found to be endowed with excellent charge transfer characteristics over the non-treated rGO. To monitor the quenching process between rGO and tetrapods, the photoluminescence (PL) decay profiles of pure tetrapods and tetrapod-rGO with and without amine treatment were investigated in solution and are summarized in Figure 1e. The PL decay traces confirm stronger quenching in amine-treated tetrapod-rGO system than the non-treated rGO,

which implies faster electron transfer from the tetrapod to rGO interface. It should be noted that the charge transfer processes happen in a wide range of times scales while PL decay analysis mainly captures those events which occur on a nanosecond time scale.

Ultrafast femtosecond pump–probe studies were utilized next to probe the existence of interfacial charge transfer processes which occur primarily in the picosecond time scale. The normalized decay profiles following the 400 nm laser pulse excitation of tetrapod films, amine-treated tetrapod-rGO films and non-treated tetrapod-rGO films are shown in Figure 1f. All decay traces are well fitted to the single exponential kinetics using Equation (1).

$$F(t) = \alpha e^{-t/\tau} \quad (1)$$

The single exponential behavior suggests that negligible Auger recombination occurs in our samples.[17] The exponential decay traces indicate the transient bleaching recovery lifetime τ of tetrapod (710 ps) is decreased when it is anchored on either pristine rGO (435 ps) or amine-treated rGO (376 ps). Based on Equation 2 below and bleaching recovery lifetime values, the relative rate for the electron transfer from tetrapod to rGO can be estimated and compared.

$$K_{et} = \frac{1}{\tau_{rGO-Tetrapod}} - \frac{1}{\tau_{Tetrapod}} \quad (2)$$

The relative electron transfer rate in the amine-treated tetrapod-rGO system is much faster than the non-treated tetrapod-rGO system, which confirms efficient charge injection from excited tetrapods into rGO. These results suggest that amine-treated rGO can act as an electron acceptor system for collecting and transporting photo-generated electrons from the tetrapod.

To ensure also efficient hole transportation in the photoactive layer, the tetrapod-rGO was blended with the polycarbazole-based conjugated polymer Poly[[9-(1-octylnonyl)-9H-carbazole-2,7-diyl]-2,5-thiophenediyl-2,1,3-benzothiadiazole-4,7-diyl-2,5-thiophenediyl] (PCDTBT), which has been widely utilized as an electron donor in organic photovoltaic devices due to its deep HOMO energy level and good atmospheric stability.[18] It is known that the internal energy loss due to carrier recombination can be partly ascribed to non-uniform surface structure, thus the surface morphology and interfacial contact between PCDTBT and tetrapod-rGO was imaged using AFM. The morphological change of the PCDTBT:tetrapod-rGO blends can be visualized in **Figure 2**a–e. The corresponding root mean square roughness (R_{rms}) values are summarized in Figure 2f.

As shown from Figure (2)a, the presence of very large polymer domains (bright regions in the plane view) in the film cast from 1:1 PCDTBT:tetrapod-rGO blend solution reflect that large scale phase separation exists within the blends. Increasing the blend ratio of PCDTBT:tetrapod-rGO to 1:7 improves mixing, and a homogeneous surface structure was obtained. Figure 2d shows the 3-D AFM image of a 1:7 PCDTBT:tetrapod-rGO blend where the smoothest surface (R_{rms} is 1 nm) is achieved among all the blended films. Further increasing the blend ratio of PCDTBT:tetrapod-rGO to 1:9 reveals dark regions that may be ascribed to a high concentration of interpenetrated tetrapod-rGO networks within the blend.

Figure 3a shows the absorption spectra of films coated from solutions of pure PCDTBT, tetrapod-rGO and blends of all three components (1:1 to 1:9 weight ratio of PCDTBT:tetrapod-rGO). Detailed preparation procedures can be found in the

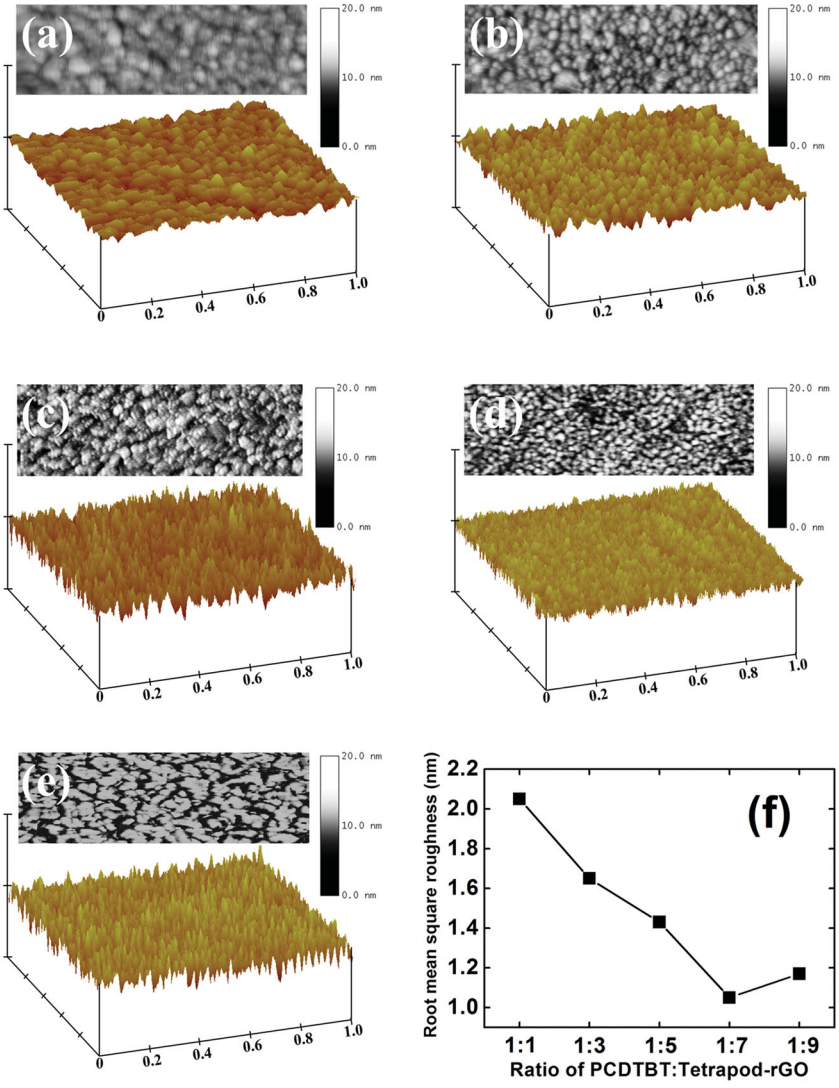

Figure 2. Morphologies of the hybrid films fabricated from different PCDTBT:tetrapod-rGO blend ratios: (a–e) 1:1, 1:3, 1:5, 1:7, and 1:9, respectively, with plane view and 3D view of an area of 1 × 1 μm^2 AFM. All films are annealed at 150 °C for 10 min. (f) Corresponding root-mean-square roughness values are plotted.

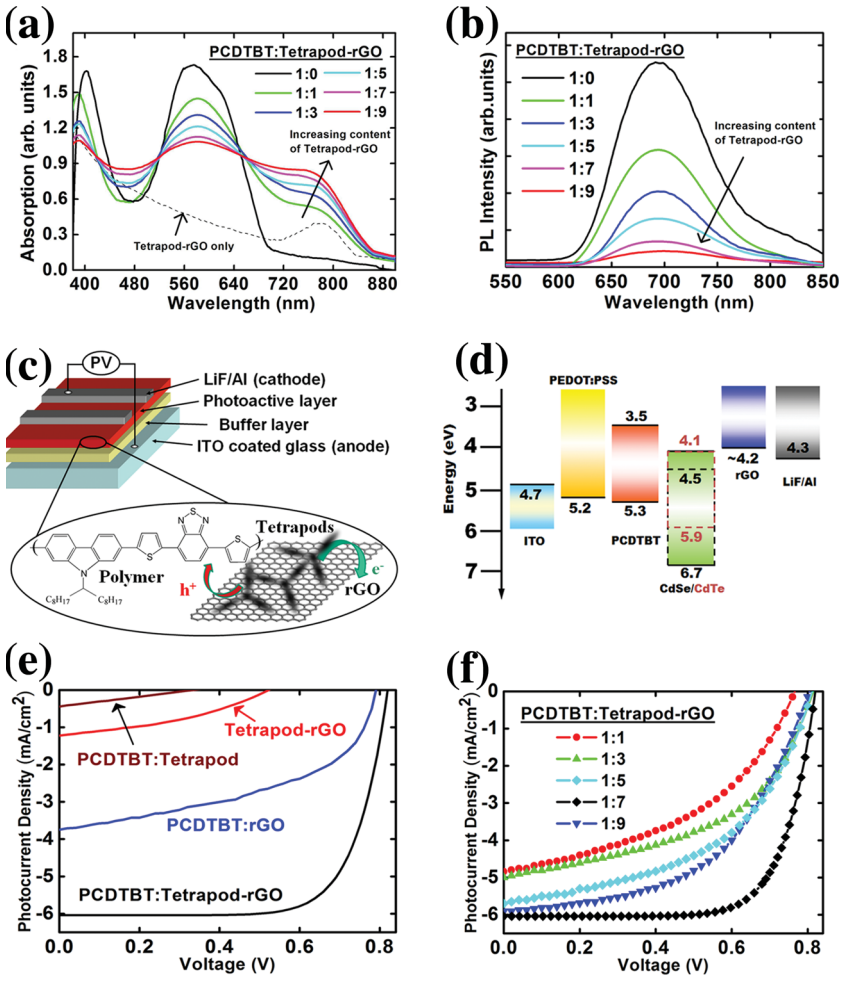

Figure 3. (a,b) Absorption and PL spectra of thin films comprising PCDTBT and Tetrapod-rGO in different blend ratio. (c) Photovoltaic device configuration used in the current study. (d) Schematic energy level diagram of the device. *J-V* characteristics of the devices with (e) different photoactive layer and (f) PCDTBT:Tetrapod-rGO in various blend ratio under light illumination intensity of 100 mW/cm^2.

experimental section. The complementary absorption spectra from the UV to NIR region (380–830 nm) are due to the overlapped optical absorption of the PCDTBT:tetrapod-rGO blends which exhibit three distinct absorption bands. Increasing the ratio of PCDTBT:tetrapod-rGO from 1:1 to 1:9 shows increased absorption in the near infrared region (wavelength at 788 nm). Steady-state PL spectra exhibit a prominent PL quenching of PCDTBT with increasing tetrapod-rGO content (Figure 3b). This result proves that the photoinduced charge carriers in the polymer can be efficiently separated via the tetrapod-rGO interface.

Figure 3c shows the photovoltaic device configuration utilized in the current study. The photoactive layer of PCDTBT:tetrapod-rGO is sandwiched between PEDOT:PSS-coated ITO and LiF/Al cathode. Three references devices which include PCDTBT:tetrapod, tetrapod-rGO and PCDTBT:rGO photoactive layers were also fabricated, respectively. The photocurrent density-voltage (*J-V*) behavior and main photovoltaic parameters of all devices are shown in Figure 3e and **Table 1**, respectively. The device with a photoactive layer of PCDTBT:tetrapod-rGO demonstrates outstanding photovoltaic performance with a high open-circuit voltage (V_{oc}) of 0.82 V, short-circuit current density (J_{sc}) of 6.04 mA/cm^2, fill factor (FF) of 0.59, and yielded a high PCE of 3.3%. The detailed origin of photocurrent generation can refer to the external quantum efficiency (EQE) of individual hybrid solar cells (supporting information). In contrast, the reference devices made with the PCDTBT:tetrapod, tetrapod-rGO and PCDTBT:rGO photoactive layer exhibited a much lower PCE of 0.04%, 0.29%, and 1.43%, respectively. These prove convincingly that all three components in PCDTBT:tetrapod-rGO blended film are essential to achieve an efficient photovoltaic effect. It must be pointed out that the uniform attachment of tetrapods on rGO is essential for achieving good photovoltaic response. For blends without amine treatment, the resultant films could only display very poor device performance with a PCE of 0.95% (not shown here).

The dramatic photovoltaic improvement in our current PCDTBT:tetrapod-rGO device is attributed to several factors. The integrated tetrapod-rGO architecture constitute a network of interpenetrating layers which are spatially and electrically continuous. This is in turn intimately contacted by the continuous PCDTBT polymer, thus ensuring efficient separation of electron and hole. The efficiency of a nanocrystal-based device is strongly governed by charge hopping or tunneling; typically, nanocrystals must be packed very closely in order to induce good percolation pathways. A common method to improve the interconnections between nanocrystals is a high temperature sintering process (400 °C) as reported by I. Gur et al.[19] Here, the PCDTBT:tetrapod-rGO blend can have a bicontinuous nanoscaled morphology (for both hole and electron transport) without high temperature treatment. Only a mild thermal annealing (150 °C) was employed to ensure the removal of any organic impurities in the coated photoactive layers. Such a low temperature thermal

Table 1. Main photovoltaic parameters extracted from the devices consisted of different photoactive materials. R_{series} is evaluated from the inverse slope of dark current-voltage characteristics of the photovoltaic device.

Photoactive material	V_{oc} [V]	J_{sc} [mA/cm^2]	FF	η [%]	R_{series} [Ωcm^2]
PCDTBT:tetrapod	0.32	0.41	0.27	0.04	1039
tetrapod-rGO	0.52	1.22	0.45	0.29	788
PCDTBT:rGO	0.78	3.84	0.49	1.43	136
PCDTBT:tetrapod-rGO	0.82	6.04	0.59	3.27	9.2

Table 2. Main photovoltaic parameters extracted from the devices with different blend ratio of PCDTBT and tetrapod-rGO. R_{series} is evaluated from the inverse slope of dark current-voltage characteristics of the photovoltaic device.

PCDTBT: tetrapod-rGO	V_{oc} [V]	J_{sc} [mA/cm^2]	FF	η [%]	R_{series} [Ωcm^2]
1:1	0.77	4.84	0.45	1.64	50.8
1:3	0.80	5.01	0.49	1.99	25.7
1:5	0.81	5.70	0.52	2.47	12.6
1:7	0.82	6.04	0.59	3.27	9.2
1:9	0.80	5.89	0.50	2.30	15.9

post-treatment is compatible with the fabrication processes of plastic electrodes for flexible solar cells. For comparison, the photovoltaic characteristic of the device with PCDTBT:CdTe Tetrapod-rGO under light illumination intensity of 100 mW/cm^2 was recorded (supporting information). The device with CdTe tetrapods only shows moderate PV efficiency of 1.4% in contrast to device with type II CdSe/CdTe tetrapods (~3.3%). The results affirm that type II band offset affords spatial separation of photogenerated carriers and thus facilitates the charge separation process and increases device efficiency.

It is worth commenting that the blend made from PCDTBT:rGO has a fair PV performance with a PCE of 1.43%. The major bottleneck is the inability to harvest photons from the near infrared region. As depicted in Figure 3d, the energy level of CdSe/CdTe tetrapod shaped nanocrystal[20] has favorable energy level alignment with the highest occupied molecular orbital of PCDTBT (5.3 eV) and the work function of rGO (~4.2 eV). The interfacial morphology of the donor/acceptor (D/A) pair is also a crucial factor affecting photovoltaic behavior. As shown by the interface morphology in Figure 2, this factor has a strong correlation with the blend ratio of PCDTBT:tetrapod-rGO and careful optimization is required for good photovoltaic performance, as shown in Figure 3f and **Table 2**. The highest PCE is achieved from the device with blends cast from a 1:7 PCDTBT:tetrapod-rGO solution. This is attributed to the largest values in the J_{sc} and the FF, compared with other blend ratios. The smooth morphology of the 1:7 PCDTBT:tetrapod-rGO blend film also results in the smallest series resistance (R_{series} is 9.2 Ωcm^2, Table 2). In addition, the nanoscaled phase separation in the optimized blend enlarges the D/A interface and facilitates the exciton dissociation process.

3. Conclusions

A high performance hybrid photovoltaic device is demonstrated combining the photoactive components of PCDTBT polymer, CdSe/CdTe tetrapods and rGO to form dispersed heterojunctions. More than twofold increment in efficiency is attained in this hybrid device over either polymer-rGO, polymer-nanocrystal, or nanocrystal-rGO devices. Chemically mediated control of nanoscale blend morphologies, for example by oleylamine treatment in this case, is found to be crucial in allowing homogeneous intermixing and allows performance bottlenecks to be breached in hybrid solar cells. The current approach in using amine-treated rGO for immobilizing nanocrystals and preventing aggregation should be applicable to a wide range of inorganic nanocrystals, and can be used for high concentration mixing of various nanocrystals in organic material for high efficiency hybrid solar cell devices.

4. Experimental Section

Synthesis of Reduced Graphene Oxide (rGO): Graphene oxide was prepared based on modified Hummers method. Initially, graphite flakes (1.5 g) were stirred in an ice bath. Sodium nitrate (1.5 g) and concentrated sulphuric acid (69 mL) were then added slowly with vigorous stirring while maintaining the mixture at 0–5 °C. After that, potassium permanganate (9 g) was added very slowly over 2 h. Then, the mixture was transferred to a 35 °C water bath and stirred for about 1 h to form a thick green paste. Following, deionized (DI) water (120 mL) was added very slowly and the mixture was stirred for another 1 hour while the temperature was raised to 90 °C. Deionized water (300 mL) was added, followed by slow addition of 30% hydrogen peroxide (9 mL). The suspension was filtered and re-dispersed in DI water. Finally, the material is repeatedly washed with DI water by centrifugation until the pH of the supernatant is around 7. The GO was then dried (1 g) and then added into 70% HNO_3 solution (200 mL). The solution was sonicated at 60 °C for 4 h. After that, the mixture was cooled and diluted with deionized (DI) water (800 mL). The solution was centrifuged at 15 000 rpm to remove the acid. The pellet product was further dialyzed in a dialysis bag for 3 days. The result material was then dried in a vacuum desiccator and stored at ambient environment. GO was reduced to rGO by thermal treatment at 600 °C in oven under hydrogen atmosphere.

Preparation of Oleylamine-Functionalized rGO: Typically, 50 mg rGO was dispersed in 5 mL oleylamine (OLA) by ultrasonication to give a well-dispersed solution. After that, 20 mL 1,2-dichlorobenzene (ODCB) was added into the solution and the mixture was centrifuged at 14 000 rpm to remove the free oleylamine (the pellet was further washed with OLA by centrifugation for 4 times). The amine-functionalized rGO could be well-dispersed in ODCB.

Chemicals Used for Tetrapod Shaped Nanocrystals: Cadmium oxide (CdO, 99.5%), octyalamine (OA, 90%), 1-octadecene (ODE, 90%), sulfur (S, reagent grade), selenium (Se, 99.99%), oleic acid (OA, 90%), myristic acid (MA, 99%), trioctylphosphine oxide (TOPO, 90%), 1-octadecene (90%), oleic acid (90%), and oleylamine (technical grade, 70%) were purchased from Sigma Aldrich. Trioctylphosphine (TOP, 97%) was purchased from Alfa Aesar. n-Octadecylphosphonic acid (ODPA, 97%), trioctylphosphine oxide (TOPO, 99%), and n-hexylphosphonic acid (HPA, 97%) were purchased from Strem. All chemicals were used without further purification.

Synthesis of Spherical Zinc Blende CdSe Seeds: Nearly monodisperse zb-CdSe nanocrystals (NCs) were synthesized via a previously reported method.[21] In a 50 mL three-neck round bottom flask 0.3 mmol CdO, 0.6 mmol myristic acid and 5 mL of 1-ODE were degassed at 90 °C for about 1 h. The solution was then heated to 250 °C for ~10–15 min to yield a clear solution, followed by the addition of 12 mL of ODE before cooling to 90 °C to degas for another 1 h. Upon cooling to room temperature, 0.012 g (0.15 mmol) of 100 mesh Se powder (99.999%) was added to the reaction mixture and degassed at 50 °C for ~20 min. Upon heating to 240 °C under N_2, a color change from colorless to yellow at ~150 °C and then to orange-red color upon reaching 240 °C were observed, signifying the formation of zb-CdSe nuclei. A degassed mixture of 0.5 mL oleic acid and 0.5 mL oleylamine in 2 mL of 1-ODE was subsequently added dropwise to the reaction mixture. As a guideline, the growth time for a ~4 nm diameter NC was approximately 2 h. As-synthesized zb-CdSe NCs were precipitated out from the growth solution by adding acetone, and were subsequently allowed to undergo two more cycles of re-dispersion and precipitation in toluene and methanol respectively.

Synthesis of CdSe Seeded CdTe Tetrapods: CdSe seeded CdTe tetrapods were synthesized via a previously reported method with slight modifications.[14] For a typical synthesis of tetrapods, 99% TOPO (3.0 g), ODPA (0.290 g), HPA (0.080 g), oleic acid (0.5 mL), and CdO (0.060 g) were mixed in a 50 mL flask. After the flask was degassed under vacuum for ~1 h at 150 °C, the resulting solution was heated to 320 °C under nitrogen to yield a colorless, clear solution. At this point, 1.8 mL of TOP was injected into the flask, and the temperature was allowed to recover to the value required for the synthesis. The mixture of precursors and CdSe nanocrystal seeds was prepared by mixing a specified amount of sulfur (or tellurium or selenium) stock solution with the solution of CdSe seeds (around 20 µL of a ~100 µM solution of CdSe). This solution was quickly injected into the flask, and then the system was allowed to react for a given time. The final sample was washed by repeated cycles of precipitation and re-dispersion via the addition of methanol and toluene respectively.

Ligand Exchange to Amine-Capped CdSe/CdTe Tetrapods: Approximately 30 nm long Zb-CdSe seeded CdTe tetrapods synthesized using ODPA and HPA were processed from growth solution and heated at 90 °C with stirring for ~24 h in the presence of excess oleylamine in toluene. Upon completion of the reaction time the resulting amine-capped tetrapods were processed at least 4 times to ensure the removal of any unbound ligand.

Preparation of Blend Films Consisting of PCDTBT:Tetrapod-rGO: Tetrapod-rGO solution was prepared by mixing amine-functionalized rGO with amine-capped tetrapods in a fixed weight ratio of 1:50. The blend films of PCDTBT:tetrapod-rGO in different weight ratio (1:1, 1:3, 1:5, 1:7, and 1:9) were deposited by spin coating from ODCB. For examples, blend ratio of 1:7 represents to mix 7 mg/mL PCDTBT to 49 mg/mL tetrapod-rGO.

Preparation of Blend Films Consisting of PCDTBT:Tetrapod, Tetrapod-rGO, and PCDTBT:rGO for Photovoltaic Devices: All films are spin coated from ODCB under different concentration. For PCDTBT:tetrapod: 7mg/mL of PCDTBT was mixed with 49 mg/mL of tetrapods. For tetrapod-rGO, 0.98 mg/mL of rGO was mixed with 49 mg/mL of tetrapods. For PCDTBT:rGO, 7 mg/mL was mixed with 0.98 mg/mL of rGO. All solutions are stirred overnight over 48 h inside glove box.

PL Decay Measurements: PL decay profiles were measured by exciting tetrapod-rGO samples with femtosecond laser pulses, generated by a mode-locked Ti:Sapphire laser seeded Ti:Sapphire regenerative amplifier (COHERENT, Vitesse). BBO crystal (SHG) was used to generate 400 nm wavelength, for the excitation. The incident laser pulses were focused by a 10 cm focal length lens (fluence ~0.3 J/cm^2, spot size ~30 µm) onto a 1 cm-thick quartz cell containing tetrapod-rGO solution. The PL signal was collected in the perpendicular direction of the incident light using a collection system of two 10 cm focal length lenses coupled in to silicon fast photodiode (EOT, Silicon PIN detector ET-2040) which was input to an oscilloscope (CRO, Tektronix TDS 380, 50-ohm-terminated, 400-MHz bandwidth).

Femtosecond Pump–Probe Studies: The experiments were carried out with femtosecond laser pulses, which were generated by a mode-locked Ti: Sapphire laser seeded Ti: Sapphire regenerative amplifier (COHERENT, Vitesse). The laser wavelength, pulse duration and repetition rate were 800 nm, 100 fs, and 1 kHz, respectively. A second harmonic crystal (BBO) was also used in the pump beam to generate laser pulses at 400 nm wavelength. The laser pulses were focused onto a 1-mm-thick quartz cuvette which contained the tetrapod-rGO solution with a minimum beam waist of 30 µm. Pump pulses were delayed using a computer controlled translation stage. Probe transmission signals were collected using Si photodiode with respect to pump delay. Pump and probe beams were cross polarized, linear transmittance of all the samples was adjusted to be 80% at 800 nm.

Fabrication of PV Devices: All substrates used in this study were cleaned with detergent, deionized water, acetone and isopropanol for 15 min. Poly(3,4-ethylenedioxythiophene):poly(styrene sulfonate) (PEDOT:PSS) was purchased from H. C. Starck. GmbH (Baytron P VP AI4083) is used as buffer layer. PEDOT:PSS film was firstly spin coated on the top of the ITO anode and dried at 100 °C for 15 min. All photoactive layers (PCDTBT:tetrapod-rGO, PCDTBT:tetrapod, tetrapod-rGO and PCDTBT:rGO) were then spin coated from ODCB on the PEDOT:PSS layer. The samples were then annealed at 150 °C for 10 min. LiF/Al cathode was thermally evaporated through a shadow mask giving an active device area of 0.04 cm^2. The fabricated solar cells were characterized with a 150 W solar simulator with AM 1.5G filter from Newport Corporation at an intensity of 100 mW/cm^2. Previously, Shrotriya et al. had reported the importance of selecting an appropriate reference cell for illumination intensity calibration.[22] In order to report a reliable device efficiency value, we used a thermal detector with same spectral responsivity profile as that used in the work of Shrotriya et al. and the spectral mismatch was corrected.

Supporting Information

Supporting Information is available from the Wiley Online Library or from the author.

Acknowledgements

The authors acknowledge funding support from the Singapore-Berkeley Research Initiative for Sustainable Energy (SinBeRISE) CREATE Program. K.P.L. acknowledges MOE AcRF Tier 2 grant "Interface Engineering of Graphene Hybrids for Energy Conversion" (R-143–000–488–112).

Received: August 28, 2013
Revised: October 6, 2013
Published online: November 19, 2013

[1] S. Kim, B. Fisher, H.-J. Eisler, M. Bawendi, *J. Am. Chem. Soc.* **2003**, *125*, 11466.
[2] J. Tang, K. W. Kemp, S. Hoogland, K. S. Jeong, H. Liu, L. Levina, M. Furukawa, X. Wang, R. Debnath, D. Cha, K. W. Chou, A. Fischer, A. Amassian, J. B. Asbury, E. H. Sargent, *Nat. Mater.* **2011**, *10*, 765.
[3] S. Stankovich, D. A. Dikin, G. H. B. Dommett, K. M. Kohlhaas, E. J. Zimney, E. A. Stach, R. D. Piner, S. T. Nguyen, R. S. Ruoff, *Nature* **2006**, *442*, 282.
[4] X. Geng, L. Niu, Z. Xing, R. Song, G. Liu, M. Sun, G. Cheng, H. Zhong, Z. Liu, Z. Zhang, L. Sun, H. Xu, L. Lu, L. Liu, *Adv. Mater.* **2010**, *22*, 638; I. V. Lightcap, P. V. Kamat, *J. Am. Chem. Soc.* **2012**, *134*, 7109; C. X. Guo, H. B. Yang, Z. M. Sheng, Z. S. Lu, Q. L. Song, C. M. Li, *Angew. Chem. Int. Ed.* **2010**, *49*, 3014.
[5] J. Chen, F. Xu, J. Wu, K. Qasim, Y. Zhou, W. Lei, L. T. Sun, Y. Zhang, *Nanoscale* **2012**, *4*, 441.
[6] J. Y. Lek, Y. M. Lam, J. Niziol, M. Marzec, *Nanotechnology* **2012**, *23*, 315401.
[7] Y. Zhou, Y. Li, H. Zhong, J. Hou, Y. Ding, C. Yang, Y. Li, *Nanotechnology* **2006**, *17*, 4041.
[8] J. M. Lee, B.-H. Kwon, H. I. Park, H. Kim, M. G. Kim, J. S. Park, E. S. Kim, S. Yoo, D. Y. Jeon, S. O. Kim, *Adv. Mater.* **2013**, *25*, 2011.
[9] M. M. Stylianakis, E. Stratakis, E. Koudoumas, E. Kymakis, S. H. Anastasiadis, *ACS Appl. Mater. Interfaces* **2012**, *4*, 4864.
[10] J. Wang, Y. Wang, D. He, Z. Liu, H. Wu, H. Wang, P. Zhou, M. Fu, *Solar Energy Mater. Solar Cells* **2012**, *96*, 58.
[11] P. A. Troshin, H. Hoppe, J. Renz, M. Egginger, J. Y. Mayorova, A. E. Goryachev, A. S. Peregudov, R. N. Lyubovskaya, G. Gobsch, N. S. Sariciftci, V. F. Razumov, *Adv. Funct. Mater.* **2009**, *19*, 779.
[12] D. Milliron, S. M. Hughes, Y. Cui, L. Manna, J. Li, L. W. Wang, A. P. Alivisatos, *Nature* **2004**, *430*, 190.
[13] S. H. Wei, S. B. Zhang, A. Zunger, *J. Appl. Phys.* **2000**, *87*, 1304.

[14] A. Fiore, R. Mastria, M. G. Lupo, G. Lanzani, C. Giannini, E. Carlino, G. Morello, M. De Giorgi, Y. Li, R. Cingolani, L. Manna, *J. Am. Chem. Soc.* **2009**, *131*, 2274.
[15] L. Zhang, J. Liang, Y. Huang, Y. Ma, Y. Wang, Y. Chen, *Carbon* **2009**, *47*, 3365.
[16] X. Li, Y. Jia, A. Cao, *ACS Nano* **2010**, *4*, 506.
[17] a) M. Zavelani-Rossi, M. G. Lupo, F. Tassone, L. Manna, G. Lanzani, *Nano Lett.* **2010**, *10*, 3142; b) F. Scotognella, K. Miszta, D. Dorfs, M. Zavelani-Rossi, R. Brescia, S. Marras, L. Manna, G. Lanzani, F. Tassone, *J. Phys. Chem. C* **2011**, *115*, 9005.
[18] a) S. H. Park, A. Roy, S. Beaupré, S. Cho, N. Coates, J. S. Moon, D. Moses, M. Leclerc, K. Lee, A. J. Heeger, *Nat. Photonics* **2009**, *3*, 297; b) S. Wakim, S. Beaupré, N. Blouin, B. R. Aich, S. Rodman, R. Gaudiana, Y. Tao, M. Leclerc, *J. Mater. Chem.* **2009**, *19*, 5351.
[19] I. Gur, N. A. Fromer, M. L. Geier, A. P. Alivisatos, *Science* **2005**, *310*, 462.
[20] Y. Li, R. Mastria, A. Fiore, C. Nobile, L. Yin, M. Biasiucci, G. Cheng, A. M. Cucolo, R. Cingolani, L. Manna, G. Gigli, *Adv. Mater.* **2009**, *21*, 4461.
[21] Y. A. Yang, H. Wu, K. R. Williams, Y. C. Cao, *Angew. Chem. Int. Ed.* **2005**, *44*, 6712.
[22] V. Shrotriya, G. Li, Y. Yao, T. Moriarty, K. Emery, Y. Yang, *Adv. Funct. Mater.* **2006**, *16*, 2016.v